

# Formation of Magnetically Truncated Accretion Disks in 3D Radiation-Transport Two-Temperature GRMHD Simulations

M.T.P. LISKA,<sup>1</sup> G. MUSOKE,<sup>2</sup> A. TCHEKHOVSKOY,<sup>3</sup> O. PORTH,<sup>2</sup> AND A. M. BELOBORODOV<sup>4,5</sup>

<sup>1</sup>*Institute for Theory and Computation, Harvard University, 60 Garden Street, Cambridge, MA 02138, USA*

<sup>2</sup>*Anton Pannekoek Institute for Astronomy, University of Amsterdam, Science Park 904, 1098 XH Amsterdam, The Netherlands*

<sup>3</sup>*Center for Interdisciplinary Exploration & Research in Astrophysics (CIERA), Physics & Astronomy, Northwestern University, Evanston, IL 60202, USA*

<sup>4</sup>*Physics Department and Columbia Astrophysics Laboratory, Columbia University, 538 West 120th Street, New York, NY 10027, USA*

<sup>5</sup>*Max Planck Institute for Astrophysics, Karl-Schwarzschild-Str. 1, D-85741, Garching, Germany*

## ABSTRACT

Multi-wavelength observations suggest that the accretion disk in the hard and intermediate states of X-ray binaries (XRBs) and active galactic nuclei (AGN) transitions from a cold, thin disk at large distances into a hot, thick flow close to the black hole. However, the formation, structure and dynamics of such truncated disks are poorly constrained due to the complexity of the thermodynamic, magnetic, and radiative processes involved. We present the first radiation-transport two-temperature general relativistic magnetohydrodynamic (GRMHD) simulations of truncated disks radiating at  $\sim 35\%$  of the Eddington luminosity with and without large-scale poloidal magnetic flux. We demonstrate that when a geometrically-thin accretion disk is threaded by large-scale net poloidal magnetic flux, it self-consistently transitions at small radii into a two-phase medium of cold gas clumps floating through a hot, magnetically dominated corona. This transition occurs at a well-defined truncation radius determined by the distance out to which the disk is saturated with magnetic flux. The average ion and electron temperatures in the semi-opaque corona reach, respectively,  $T_i \gtrsim 10^{10} K$  and  $T_e \gtrsim 5 \times 10^8 K$ . The system produces radiation, powerful collimated jets and broader winds at the total energy efficiency exceeding 90%, the highest ever energy extraction efficiency from a spinning black hole by a radiatively efficient flow in a GRMHD simulation. This is consistent with jetted ejections observed during XRB outbursts. The two-phase medium can naturally lead to broadened iron line emission observed in the hard state.

## 1. INTRODUCTION

Observations spanning the radio to gamma-ray frequency range show that black hole (BH) X-ray binaries (XRBs) cycle through different spectral states of accretion over the course of months to years (e.g. Esin et al. 1997; Remillard & McClintock 2006). BH XRBs spend most of their time in a dim, quiescent state. However, from time to time they go into outburst during which they transition into orders of magnitude more luminous spectral states some of which are associated with powerful collimated outflows, or jets. During such spectral state transitions, the spectrum of the source changes from a power-law-like ‘hard’ spectrum to a blackbody-like ‘soft’ spectrum. During the outbursts, the accretion rate  $\dot{M}$  can reach a substantial fraction of the Eddington limit,  $\dot{M}_{Edd}$ , at which the radiation forces become comparable with gravity. In fact, it is conceivable that most black hole growth occurs during outbursts when the disk is most

luminous (e.g. Volonteri et al. 2007). In particular, the ‘luminous-hard state’ is very interesting since it is associated with the most powerful transient jets in XRBs (e.g., Fender et al. 2004a) and Fanaroff-Riley type 2 (FR II, Fanaroff & Riley 1974) jets in luminous AGN (e.g. Tchekhovskoy 2015; Davis & Tchekhovskoy 2020).

Accretion disks are generally described by either a geometrically-thin, optically-thick disk (Shakura & Sunyaev 1973; Novikov & Thorne 1973) or a geometrically-thick, optically-thin radiatively inefficient accretion flow (RIAF) such as an advection dominated accretion flow (ADAF, see Narayan & Yi 1994). In a geometrically-thin disk the density and optical depth are high. The balance between the radiative cooling and turbulent dissipation rates determines the geometric thickness, or the scaleheight, of the disk. Such geometrically-thin disk models can explain thermal emission in the high-soft state. In a RIAF, the density is so low that the plasma decouples into a two-temperature fluid, in which the Coulomb collisions between the ions and electrons become too rare to equilibrate the temperatures of the two species. This thermal decoupling, along with the preferential heat-

ing of the ions, prevents the disk from radiating a dynamically significant amount of dissipated energy. RIAFs can explain emission in the quiescent and hard spectral states (e.g. Abramowicz & Fragile 2013, and references therein).

When a quiescent black hole accretion system goes into an outburst, it transitions into a hybrid state that features both the thermal ‘soft’ and non-thermal ‘hard’ components in its spectrum. This suggests the presence of both a standard accretion disk and a RIAF (e.g. Remillard & McClintock 2006). In the literature, ‘truncated’ disk models form a popular paradigm describing such hybrid states (e.g. Esin et al. 1997; Ferreira et al. 2006; Done et al. 2007; Marcel et al. 2018), including their quasi-periodic variability (e.g. Ingram et al. 2009). In these truncated disk models, the outer part of the disk is geometrically-thin while the inner part is geometrically-thick, hot, and described by an RIAF. We refer to the inner, hot RIAF-like part of the system as the corona. The nature of the corona is actively debated, and its origin and geometry – often represented as a hot ‘lamppost’ – are not definitively known. The corona can Comptonize its own cyclo-synchrotron emission in addition to thermal emission from a thin accretion disk (e.g. Wardziński & Zdziarski 2000; Del Santo et al. 2013). It is important to note that the power-law emission attributed to the corona can make up a significant fraction of the total X-ray luminosity in BHXRBs and AGN and hence in such cases the hot coronal gas is likely to be also dynamically important (e.g. Reynolds & Fabian 1997; Fukumura & Kazanas 2007; Wilkins & Fabian 2012, and references therein).

A major point of contention concerns the behavior of the truncation radius,  $r_{tr}$ , which marks the transition from the outer geometrically-thin, radiatively efficient disk to the inner geometrically-thick, radiatively inefficient corona. It is not clear if the softening of the spectrum during a state transition is primarily caused by the truncation radius moving inwards (Fender et al. 2004b) or the corona shrinking in size (e.g. Kara et al. 2019), and what roles Compton-upscattered X-ray emission from the base of the jet (e.g. Markoff et al. 2005) and/or relativistic winds (Beloborodov 1999) play. In addition, the presence of broadened iron lines (e.g. Reis et al. 2010), which are typically associated with a reservoir of cold optically-thick gas near the innermost stable circular orbit (ISCO), in the low-hard state of several BHXRB systems is inconsistent with the standard picture of a truncated disk, which does not predict the presence of any cold gas within the truncation radius (e.g. Done & Gierliński 2006; Done et al. 2007).

Here, we use the state-of-the-art radiation-transport two-temperature GRMHD simulations to demonstrate that truncated accretion disks naturally form in the presence of large-scale net poloidal magnetic flux. In Sections 2 and 3 we describe our GRMHD code H-AMR and the initial conditions,

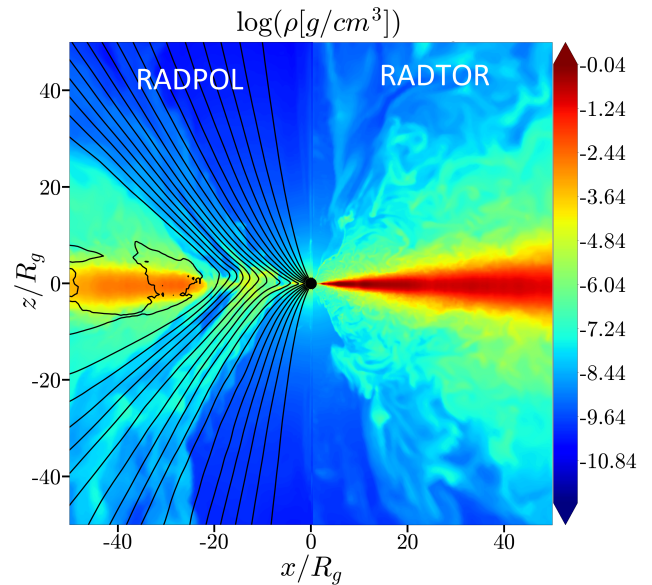


**Figure 1.** A transverse slice through density with magnetic field lines shown in black for our model with poloidal magnetic flux (RADPOL, left) and model with toroidal magnetic flux (RADTOR, right) right before enabling the radiation transport. While the RADTOR simulation forms a thin accretion disk with a constant scale-height, the inner disk in the RADPOL simulation enters the MAD state and accretion proceeds through non-axisymmetric RTI modes.

before presenting our results and concluding in Sections 4 and 5.

## 2. NUMERICAL SETUP

We use for our simulations the graphical processing unit (GPU) accelerated GRMHD code H-AMR (Liska et al. 2018b, 2019; see Porth et al. 2019 for code comparison). H-AMR is triple level parallelized using a hybrid CUDA-OpenMP-MPI framework that solves the equations of GRMHD in the Kerr-Schild foliation. Magnetic fields are evolved using a staggered grid approached based on Gardiner & Stone (2005). The spatial reconstruction of primitive variables from cell centers to cell faces is done using a third order accurate PPM method (Colella & Woodward 1984), which leads to second order overall spatial accuracy (cross-dimensional terms are not taken into account). Integration in time is performed using the second order IMEX2A scheme described in McKinney et al. (2013). H-AMR features a flexible adaptive mesh refinement (AMR) framework that allows for the refinement both in space and time. Namely, our local adaptive time-stepping approach allows different blocks to have different time steps even at the same refinement level (Liska et al. 2019).

We have recently implemented on-the-fly radiation transport into H-AMR using an M1 (two-moment) closure, following the implementations in Koral (Sądowski et al. 2013; Sądowski et al. 2017) and HARMRAD (McKinney et al.

2013). We include the energy-averaged bound-free, free-free, and cyclo-Synchrotron absorption ( $\kappa_{abs}$ ) and emission ( $\kappa_{em}$ ) opacities in addition to the electrons scattering ( $\kappa_{es}$ ) opacity as given in McKinney et al. (2017). The M1 closure works well in the optically-thick disk body and outside of the thin disk where the radiation moves predominantly in one direction (perpendicular to the disk surface), as is the case in our work. By using the energy-averaged grey-opacities we ensure that the cooling rate of the optically thin corona is as realistic as possible within the M1-framework. To approximate Compton cooling of the corona we implemented both blackbody and photon number conserving Comptonization in H-AMR (Sądowski & Narayan 2015). We discuss the validity of this method in section 5.

To allow for the development of a two-phase medium we have implemented two-temperature thermodynamics in H-AMR, and combined it with our M1 radiation scheme. In H-AMR, we evolve the ion and electron entropy tracer,  $\kappa = p_{e,i}/\rho^{\Gamma-1}$ , where  $p_{e,i}$  is the electron and ion pressure, respectively,  $\rho$  is the fluid-frame rest-mass density. In this work, we adopt  $\Gamma = 5/3$  for both electrons and ions: we have verified that this is a safe choice by carrying out simulations with variable polytropic index for the electrons. The total dissipation is calculated as the difference between the internal energies computed from the total energy equation and from the entropy tracers (Ressler et al. 2015). For the purposes of partitioning the dissipated energy between the ions and electrons, we assume here that the dissipation ultimately occurs via magnetic reconnection in unresolved current sheets. The dissipated energy is divided between the ions and electrons using an analytical prescription derived from particle-in-cell simulations (Rowan et al. 2017). We account for the energy exchange via Coulomb collisions between ions and electrons through an implicit source term (Sądowski et al. 2017). Due to the low radiative efficiency of ions as compared to electrons, when a two-temperature fluid forms, we assume that radiative cooling reduces the electron entropy and keeps the ion entropy constant.

H-AMR allows broad flexibility in the choice of a coordinate system. Here, we adopt spherical polar coordinates,  $r, \theta, \phi$ , and choose a uniform grid in the  $\log r$ ,  $\theta$ , and  $\phi$  variables. We use a base resolution of  $1020 \times 432 \times 288$  cells in the three dimensions, respectively. We then use AMR to increase this resolution in the regions of interest, as we describe below. We place the inner radial boundary inside of the event horizon (with  $\geq 5$  radial cells inside of the event horizon at the base level: this ensures that the inner radial grid boundary is properly causally-disconnected from the black hole exterior). We place the outer radial boundary at  $R_{out} = 10^4 r_g$ . To resolve the structure of the thin equatorial disk, we quadruple the resolution for  $5r_g \lesssim r \lesssim 120r_g$  within  $7.5^\circ$  of the midplane to  $4080 \times 1728 \times 1152$  cells

by adding 2 layers of static mesh refinement. In addition, we use 4 levels of local adaptive time-stepping. To prevent cell squeezing near the poles ( $\theta = 0, \pi$ ), we progressively reduce the  $\phi$ -resolution to  $N_\phi = 18$  within  $30^\circ$  from each pole (we leave the resolutions in the other two dimensions unaffected). We use outflow boundary conditions in  $r$ -, transmissive boundary conditions in  $\theta$ - and periodic boundary conditions in  $\phi$ -directions. The grid features in total  $\sim 10^9$  cells and achieves a computational speeds of effectively  $1.5 \times 10^7$  zone-cycles/s/GPU (taking into account the speedup from the local adaptive timestepping). This is an order of magnitude less compared to the non-radiative version of H-AMR.

### 3. PHYSICAL SETUP

To study the effect of large-scale magnetic flux on the structure of the inner disk, we consider two models. We initialize the model RADPOL with a purely poloidal magnetic field and model RADTOR with a purely toroidal magnetic field. Both models feature a rapidly spinning black hole of dimensionless spin  $a = 0.9375$  and use a  $\Gamma = 5/3$  for ions and electrons. Since ideal GRMHD is unable to describe the physical processes responsible for injecting gas in the jet funnel we use drift-frame density floors (Ressler et al. 2017) to ensure that  $\rho c^2 \geq p_{mag}/12.5$  in the jets.

Model RADPOL starts with a thick equatorial torus in hydrostatic equilibrium with the inner radius at  $r_{in} = 12.5r_g$ , density maximum at  $r_{max} = 25r_g$ , and outer radius  $r_{out} = 200r_g$  (Fishbone & Moncrief 1976). The magnetic field has the vector potential  $A_\phi \propto (\rho - 0.05)^2 r^2$ . We normalize this magnetic field such that  $\beta = \max p_{gas} / \max p_{mag} = 30$  where  $p_{gas}$  and  $p_{mag}$  are the gas and magnetic pressures, and ‘max’ denotes the maximum taken over the torus. This setup is intended to represent the hard intermediate state, where the outer disk is expected to collapse due to radiative cooling.

Model RADTOR starts with a thin equatorial accretion disk on Keplerian orbits in approximate hydrostatic equilibrium whose density distribution,  $\rho(r, z) \propto r^{-1} \exp(-z^2/2h^2)$ , extends from an inner radius,  $r_{in} = 6r_g$ , to the outer radius,  $r_{out} = 76r_g$  at the constant  $h/r = 0.03$ . Magnetic field is described by a vector potential  $A_\theta \propto (\rho - 0.0005)r^2$ , which is normalized to give an approximately uniform  $\beta \sim 7$ . This setup is intended to represent the high soft state, where neither large-scale poloidal magnetic flux nor jets are present, presumably because all net poloidal magnetic flux has diffused out after the disk has settled into a geometrically thin disk (e.g. Begelman & Armitage 2014).

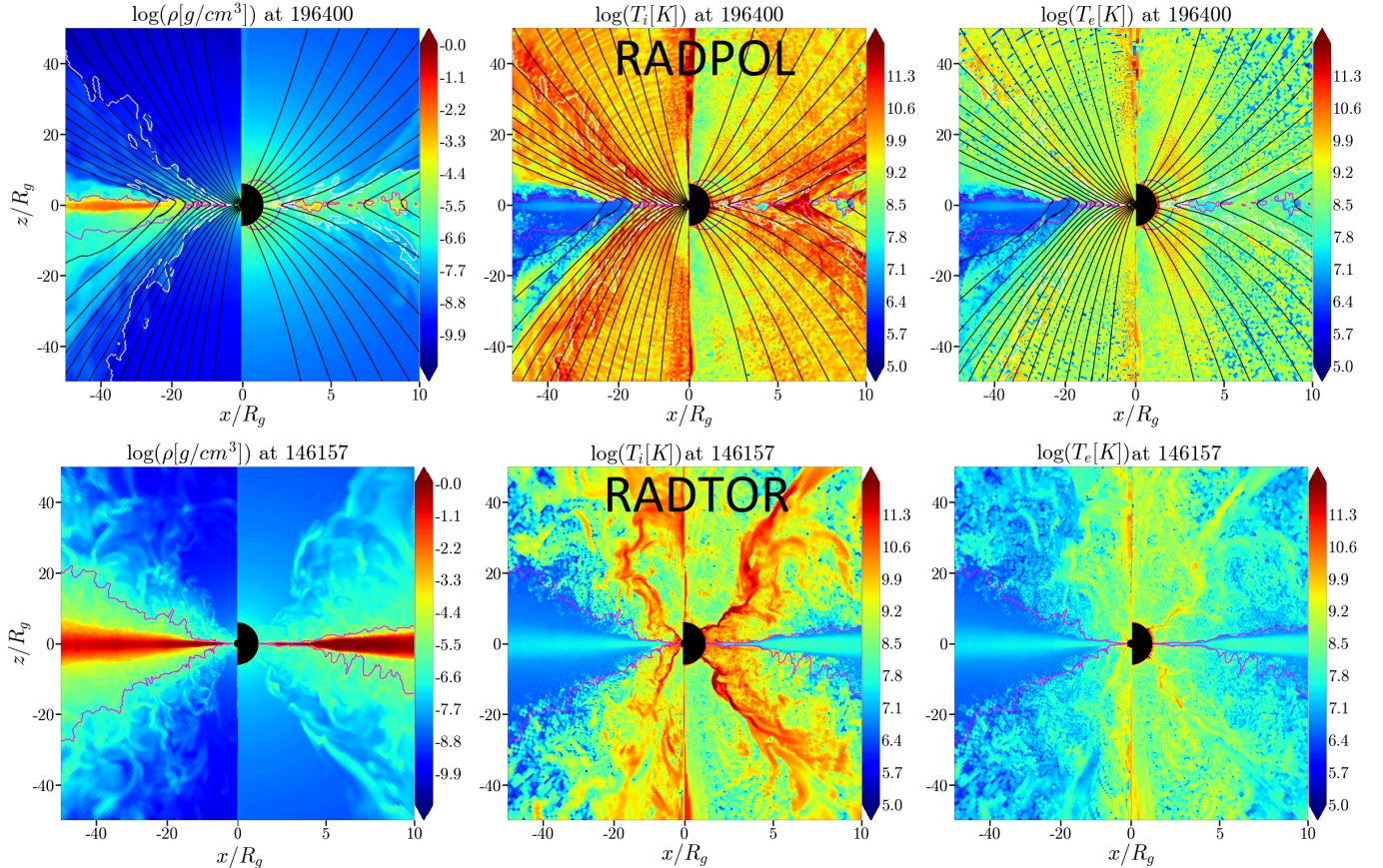


**Figure 2.** The presence of large-scale poloidal magnetic flux leads to the development of a two-phase medium: a low-density, thick, hot corona-like accretion flow with patches of cold gas floating through it (top row, model RADPOL). In contrast, in the absence of the poloidal magnetic flux the cold, thin flow extends down to the black hole (bottom row, model RADTOR). The three columns, from left to right, show vertical slices through the density, ion temperature, and electron temperature; the right hemispheres show zoom-ins on the left hemispheres. Magnetic field lines are shown in black, jet boundary in white ( $p_{\text{mag}} = \rho c^2$ ), and the last scattering surface in pink ( $\tau_{\text{es}} = 1$ , integrated in vertical direction). In RADPOL the accretion disk transitions into a magnetic pressure supported corona within  $r \lesssim 20r_g$ , which decouples into a 2-temperature plasma of hot, radiating, electrons and very hot, non-radiating, ions. Optically thick patches of cold gas cover a significant surface fraction of the corona. In RADTOR the plasma in the disk remains strongly coupled and optically thick.

#### 4. RESULTS

We evolve both models in two stages. During the first stage, we use neither the radiation transport nor two-temperature thermodynamics. Instead, we use a cooling function (Noble et al. 2009) to cool the disk to a target thermal scaleheight of  $(h/r)_{\text{init}} = 0.03$ : this cooling process takes  $\sim 10^3 r_g/c$  for RADPOL and mimics the catastrophic cooling of a BHXR disk undergoing an outburst. We initialize RADTOR at the target temperature profile corresponding to the same disk scaleheight,  $(h/r)_{\text{init}} = 0.03$ . We evolve RADPOL for  $t \sim 188,840 r_g/c$  and RADTOR for  $t \sim 136,075 r_g/c$ . The left panel in Figure 1 shows that RADPOL accumulates large-scale poloidal magnetic flux in the inner disk: this is similar to the model described in Liska et al. (2018a), which is essentially the same as RADPOL, apart from a small disk tilt, numerical grid, and duration. The flux accumulation is accompanied by a decrease in density at  $r \lesssim 20r_g$  and the development of a magnetically arrested

disk (MAD, Tchekhovskoy et al. 2011): the accretion in the inner disk proceeds through magnetic Rayleigh-Taylor instabilities (RTI), as is expected in a MAD (e.g. Tchekhovskoy et al. 2011; McKinney et al. 2012). Neither of these two effects are observed for RADTOR (right panel of Fig. 1) and highlights the importance of the net poloidal magnetic flux for driving the disk truncation.

In the second stage, we set  $M_{\text{BH}} = 10M_{\odot}$ , renormalize the density such that  $\langle \dot{M} \rangle \sim 0.35 \dot{M}_{\text{Edd}}$ , and set  $T_{\text{rad}} = T_e = T_i$ , where we define  $\dot{M}_{\text{Edd}} = L_{\text{Edd}}/\eta$  with  $\eta = \eta_{\text{NT}} = 0.178$  and  $L_{\text{Edd}} = 4\pi GM_{\text{BH}}/\kappa_{\text{es}}$ . We assume solar abundances of hydrogen, helium and metals ( $X = 0.7, Y = 0.28, Z = 0.02$ ). We then run both simulations for another  $t \sim 1.35 \times 10^4 r_g/c$  in full radiation-transport two-temperature GRMHD: for time interval  $t \in [188840, 203360] r_g/c$  in RADPOL and  $t \in [136076, 148997] r_g/c$  in RADTOR. We use blackbody Comptonization for both models, except during  $t \in [191840, 193650] r_g/c$  in RADPOL, where we use

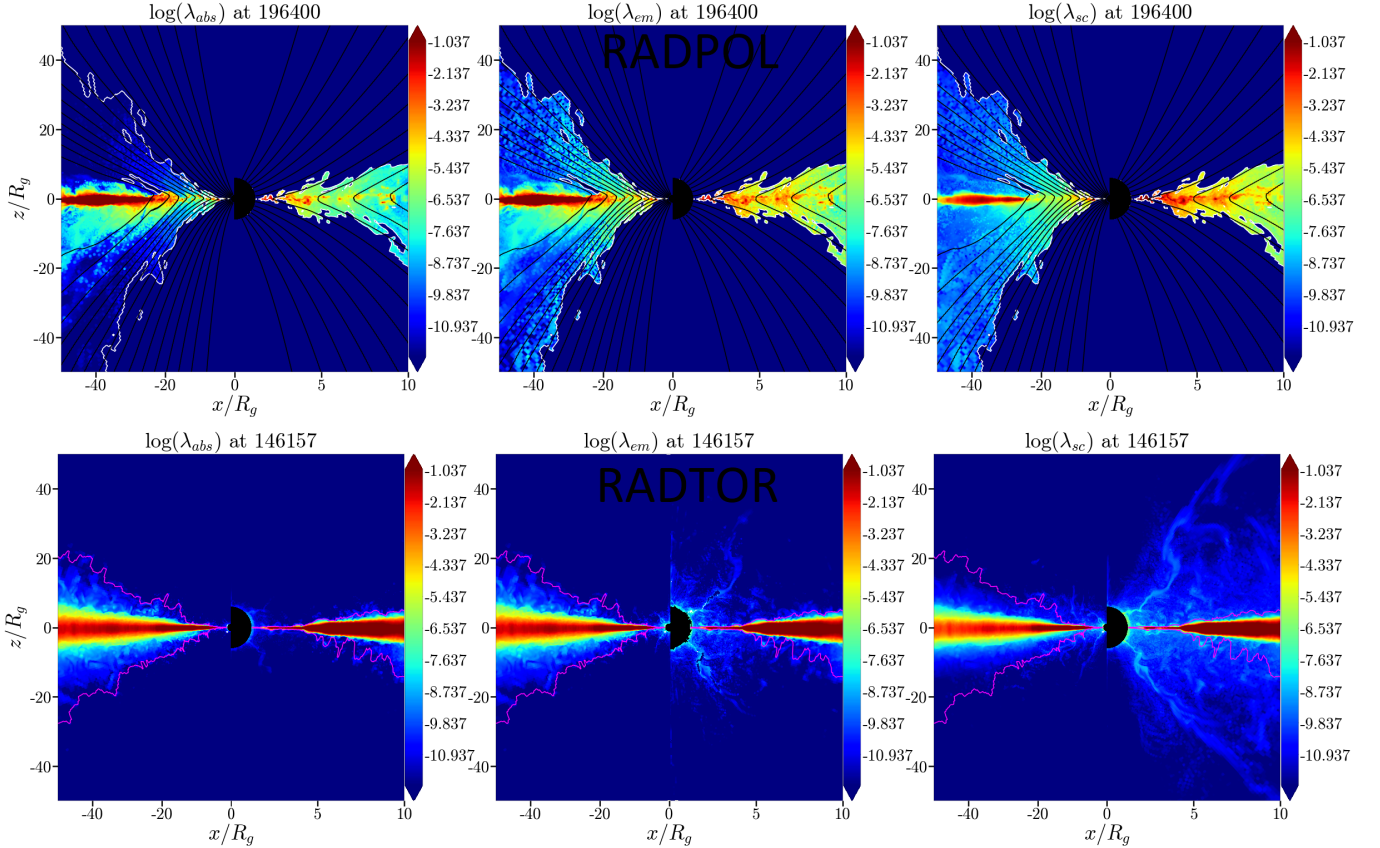


**Figure 3.** The absorption heating rate ( $\lambda_{abs}$ , left column), emission cooling rate ( $\lambda_{em}$ , middle column), and Compton cooling rate ( $\lambda_{sc}$ , right column) for models RADPOL (top row) and RADTOR (bottom row). The right hemispheres show zoom-ins of the left hemisphere. Magnetic field lines are shown in black, jet boundary in white ( $p_{mag} = \rho c^2$ ), and the last scattering surface in pink ( $\tau_{es} = 1$ , integrated in vertical direction). For clarity, we have removed data from the jet. Cooling outside of the jet in RADPOL is concentrated in the high density gas near the equatorial plane, which has electron temperatures of  $T_e \gtrsim 5 \times 10^8 K$ . Here Compton cooling clearly dominates over emission cooling, especially since a large fraction of the emitted energy gets self-absorbed. This Compton up-scattering is expected to significantly harden the spectrum. On the other hand, in RADTOR the cold ( $T_e \sim \text{few} \times 10^7 K$ ) and optically thick plasma will emit a much softer blackbody-like spectrum.

photon-number conserving Comptonization. In addition, we use for RADPOL during  $t \in [193650, 196550] r_g/c$  a lower density floor of  $\rho c^2 \geq p_{mag}/25$ . Additionally, for the time interval of  $t \in [188840, 192840] r_g/c$  in RADPOL we limit the ratio of the electron to ion temperatures to  $T_e/T_i \gtrsim 10^{-2}$  instead of the usual  $T_e/T_i \gtrsim 10^{-4}$ . These tests validate that the results presented in this article are not sensitive to the Comptonization routine employed or the value of the density floors as can be witnessed by the animations on our [YouTube channel](#). However, setting the temperature floor to  $T_e/T_i \gtrsim 0.01$  artificially increased the temperature of the electrons in the current sheet within  $r \sim 5 r_g$  of the black hole.

The top row in Figure 2 (see also our [YouTube channel](#) for animations of the figure) shows that in RADPOL the inner disk decouples into a hot, optically thin, two-temperature plasma and can thus be associated with a corona. Electrons reach temperatures of  $T_e \gtrsim 5 \times 10^8 K$  while the ions reach temperatures of  $T_i \gtrsim 10^{10} K$  irrespective of the Comptonization routine employed. Dissipation, most likely caused by magnetic reconnection in current sheets near the midplane

(e.g. [Ripperda et al. 2021](#)), leads to localised heating of the plasma to temperatures of  $T_i \sim 10^{12} K$  and  $T_e \sim 10^9 K$ , which suggest that electrons radiate their heat locally (see also [Beloborodov 2017](#)). A significant part of this heated plasma flows out as a wind along the magnetic field lines. On the other hand, pockets of cold gas survive and fall into the black hole predominantly along the equatorial plane. Figure 3 shows the cooling rate of the plasma due to emission ( $\lambda_{em} = \kappa_{em} a_{rad} T_e^4$ ) and inverse Compton scattering ( $\lambda_{sc} = \kappa_{es} E_{rad} 4k_b T_e / m_e c^2$ ), in addition to the heating rate through absorption ( $\lambda_{abs} = \kappa_{abs} E_{rad}$ ). As can be seen, the cooling is predominantly concentrated near the equatorial plane. Since the emission and absorption rates are similar, primarily due to cyclo-Synchrotron self absorption, it is conceivable that most radiation actually gets Compton up-scattered before leaving the corona. We find that the Compton- $y$  parameter ( $y = \tau_{es} 4k_b T_e / m_e c^2$ ), which measures the average fractional energy gain of photons due to Comptonization (e.g. [Rybicki & Lightman 1986](#)), can easily exceed  $y \gtrsim 1$  near the midplane of the corona. These facts suggest that the

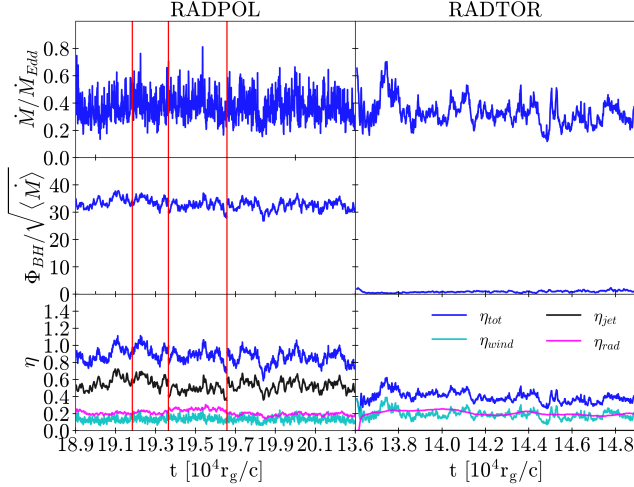


**Figure 4.** The first demonstration of highly efficient energy extraction from a rapidly spinning black hole by a radiatively efficient accretion flow in a radiation GRMHD simulation. From top to bottom, the panels show the accretion rate in Eddington units, normalized magnetic flux on black hole and outflow efficiencies (total in blue, jet in black, wind in cyan, and radiative in purple; see the legend) for the radiative stage of the simulations. Both RADPOL and RADTOR accrete at  $\dot{M}/\dot{M}_{Edd} \sim 0.35$ . The red lines demarcate the time intervals when we use either photon-conserving Comptonization ( $t \in [191840, 193650]r_g/c$ ) or a higher density floor ( $t \in [193650, 196550]r_g/c$ ). While RADPOL floods the black hole with the large-scale poloidal magnetic flux and reaches the MAD state, RADTOR does not develop any net large-scale poloidal magnetic flux. In RADPOL, the total efficiency exceeds  $\eta_{tot} \sim 90\%$ , for the first time demonstrating highly efficient energy extraction from a radiatively efficient accretion flow out of spinning black hole in a radiation GRMHD simulation. The efficiencies of the jet and winds reach respectively  $\eta_{jet} \sim 50\%$  and  $\eta_{wind} \sim 15\%$ . In contrast, in the RADTOR simulation, the total efficiency is much smaller,  $\eta_{tot} \sim 40\%$ , with a much smaller  $\eta_{jet} \lesssim 1\%$ , and approximately the same  $\eta_{wind} \sim 20\%$ . Both models achieve similar radiative outflow efficiencies,  $\eta_{rad} \sim 20\%$ .

$T_e \gtrsim 5 \times 10^8 K$  corona will up-scatter and significantly harden the radiation emitted by the cold clumps of gas in addition its own cyclo-Synchrotron emission (see also Dexter et al. 2021; Scepi et al. 2021). In contrast, the bottom row in Figure 2 shows that in RADTOR the ions and electrons are strongly coupled in the cold disk, which remains optically thick to both scattering and absorption. This suggests a strong thermal emission component. Compton up-scattering of disk photons by the winds sandwiching the inner disk is not expected since, among other things, these winds are relatively cold ( $T_e \lesssim 5 \times 10^7 K$ ), which barely exceeds the temperature of the plasma in the disk.

We show the accretion rate  $\dot{M} = -\int_0^{2\pi} \int_0^\pi \rho u^r \sqrt{-g} d\theta d\phi$ , with the integral evaluated at  $r = 5r_g$  to avoid the contamination by the density floors, and dimensionless black hole poloidal magnetic flux  $\phi_{BH} =$

$0.5 \int_0^{2\pi} \int_0^\pi |B^r| \sqrt{-g} d\theta d\phi / \langle \dot{M} \rangle^{1/2}$ , with the integral evaluated at the event horizon,  $r = r_H \simeq 1.3r_g$ , in the upper and middle panels of Figure 4. In the RADPOL model, the accretion disk transports so much of the initial poloidal magnetic flux to the black hole that it becomes as strong as gravity, obstructs the accretion, reaches a saturated value, and leads to a MAD. The normalized magnetic flux  $\phi_{BH} \sim 33$  is about two-thirds of that in thick accretion disks (Tchekhovskoy et al. 2011) and consistent with the MAD saturation value in thin accretion disks (Cheng, Liska et al 2022, in prep). The lower panel of Figure 4 shows that RADPOL launches powerful jets and winds. Namely, we show the jet ( $\eta_{jet}$ ) and wind ( $\eta_{wind}$ ) energy efficiencies, which we obtain by normalizing the electromagnetic plus fluid energy fluxes at  $r = 5r_g$  in the jets and winds by the mass accretion rate (see Liska et al. 2018a). We define the jet-wind boundary by the  $p_{mag} = \rho c^2$  criterion. In RADPOL, we find  $\eta_{wind} \sim 15\%$  and  $\eta_{jet} \sim 50\%$ . In RADTOR, we find  $\eta_{wind} \sim 20\%$  and  $\eta_{jet} \lesssim 1\%$ . In both models the associated winds are significantly hotter than the disk. We compute the radiative efficiency from the normalized radiation energy flux measured at  $r = 100r_g$  and find  $\eta_{rad} \sim 20\%$  in both models. This is remarkably close to the Novikov & Thorne (1973) value  $\eta_{NT} \sim 17.8\%$ .

As Figure 2 shows, in RADPOL the excess magnetic flux remains in the inner disk,  $r \lesssim r_{tr} \approx 20r_g$ . The left column in Figure 5 shows that this leads to the formation of a magnetic pressure supported low-density inner disk coupled to a radiation pressure supported high-density outer disk. The transition between these two regimes occurs at a well-defined ‘magnetic truncation’ radius,  $r_{tr}$ , which is set by the distance out to which the inner disk is flooded by the poloidal magnetic flux. Similar to the single-temperature simulation stage (Fig. 1), here the accretion in the inner disk also proceeds through magnetic RTI and is the radiative analog of the MAD (see also Morales Teixeira et al. 2018). On the other hand, the disk in RADTOR remains radiation pressure dominated and does not contain any large-scale poloidal magnetic flux. We define the effective viscosity as  $\alpha_{eff} = -\langle v_r v_\phi \rangle_\rho / \langle (h/r)_{in}^2 v_\phi^2 \rangle_\rho$ , where  $\langle \dots \rangle_\rho$  is the density-weighted angular average, and  $v_r$  and  $v_\phi$  are the physical radial and azimuthal velocity components, respectively. Figure 5(g,h) shows that  $\alpha_{eff} \sim 10^1$  in RADPOL and  $\alpha_{eff} \sim 10^{-2}$  in RADTOR. This illustrates that the presence of large scale magnetic flux, as in RADPOL, leads to more rapid accretion of gas (e.g. Ferreira et al. 2006).

In both models the scaleheight of the radiation pressure supported part of the disk shrinks to a density averaged scaleheight  $h/r = \langle |\theta - \pi/2| \rangle_\rho \sim 0.015 - 0.02$  (Fig. 5 panels g and h and YouTube channel) at which point we are forced to terminate the simulation since the turbulence becomes under-resolved. This runaway cooling effect suggests that both disks are subject to viscous and/or thermal instabili-

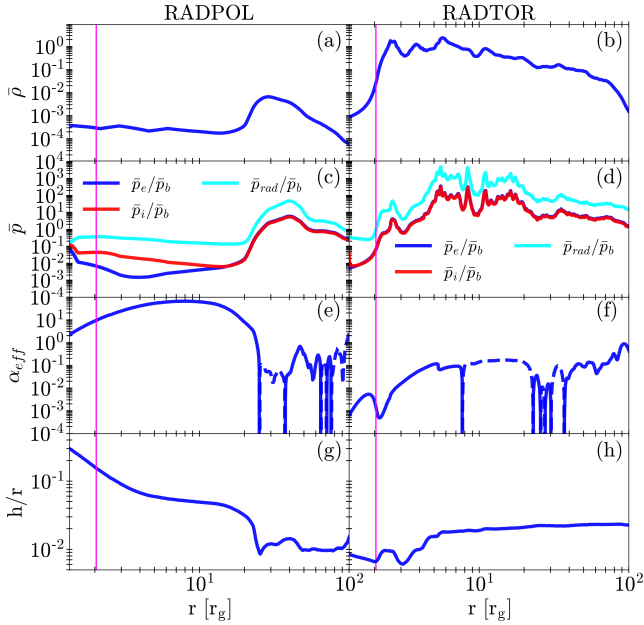


**Figure 5.** Low-density, magnetically-dominated, rapidly accreting, thicker corona-like accretion flow develops near the black hole only in the presence of large-scale poloidal magnetic flux. From top to bottom, the panels show density-averaged midplane density  $\bar{\rho} = \int \rho^2 dV / \int \rho dV$  (panels a and b); the ratios of density-averaged pressures,  $\bar{p} = \int \rho p dV / \int \rho dV$  (panels c and d); effective  $\alpha$ -viscosity (panels e and f; dashed lines indicate negative values); and scaleheights (panels g and h) time-averaged over the radiative evolution stage of the simulations. The left panels show RADPOL and right panels RADTOR results. The magenta line illustrates the location of the ISCO. While in both models the outer disk ( $r \gtrsim 20r_g$ ) is radiation pressure dominated, the inner disk in RADPOL becomes magnetic pressure dominated and forms a two-temperature plasma (with  $\bar{p}_e \ll \bar{p}_i$ ). This transition to a magnetic pressure supported corona in RADPOL is accompanied by a sharp drop in density and an increase in the effective scaleheight. The presence of large scale poloidal magnetic flux leads to rapid accretion in RADPOL as evidenced by the extremely high value of  $\alpha_{eff}$ .

ties (Lightman & Eardley 1974; Shakura & Sunyaev 1976). However, in RADPOL magnetic pressure stabilizes the inner disk against thermal collapse, which settles into a scaleheight of  $h/r \sim 0.05 - 0.2$ . Future simulations with higher resolutions and longer runtimes will investigate whether magnetic pressure or other physical processes eventually stabilize the entire accretion disk against runaway collapse (e.g. Begelman & Pringle 2007). This was suggested by radiative GRMHD simulations of thin accretion disks seeded with equipartition strength magnetic fields (e.g. Sądowski 2016; Lančová et al. 2019).

## 5. DISCUSSION AND CONCLUSION

In this work we have presented the first radiation-transport two-temperature GRMHD simulations of luminous sub-Eddington accretion disks. The simulations accrete at the

Eddington ratio  $\lambda = \langle \dot{M} \rangle / \dot{M}_{Edd} \sim 0.35$ . One of the simulations, model RADTOR, had no net poloidal magnetic flux, while the other one, model RADPOL, became saturated with poloidal magnetic flux and entered a MAD state. We demonstrated that the saturation of magnetic flux in the inner disk creates a sharp transition between a radiation pressure supported outer disk and magnetic pressure supported inner corona. The sharp transition between the two occurs at a magnetic truncation radius of  $r_{tr} \sim 20r_g$ . Powerful jets, winds, and radiative outflows with a combined efficiency of  $\eta_{tot} \gtrsim 90\%$  emerge in the presence of this poloidal magnetic flux. All of these characteristics are consistent with accretion in the hard (-intermediate state) of BHXRBs.

The corona is best described by a MAD where radial magnetic pressure gradients prevent ordered quasi-axisymmetric accretion of gas (e.g. Narayan et al. 2003; Igumenshchev et al. 2003; Igumenshchev 2008; Tchekhovskoy et al. 2011; McKinney et al. 2012; Begelman et al. 2021). Accretion of gas in the corona proceeds through magnetic RTI instabilities originating at the truncation radius. While a significant fraction of the infalling gas gets heated by magnetic reconnection to  $T_i \gtrsim 10^{10}K$  and  $T_e \gtrsim 5 \times 10^8K$ , we also observe cold, optically thick, clumps of gas falling into the black hole (Fig.2). This could potentially explain broad iron line emission observed in the hard spectral states of XRBs and AGN (e.g. Reis et al. 2010) without the need for the corona to recondense into a thin accretion disk near the black hole (e.g. Meyer-Hofmeister & Meyer 2011).

Our model differs substantially from most truncated accretion disk models in the literature (e.g. Esin et al. 1997; Ferreira et al. 2006; Begelman & Armitage 2014). In such models heat conducted from the corona into the upper layers of the disk leads to the disk's gradual evaporation into a corona (e.g. Meyer & Meyer-Hofmeister 1994; Liu & Osher 1998; Qian et al. 2007). However, in magnetically truncated disks the transition from a disk into a corona occurs at a well-defined radius which is determined by the location of the magnetospheric radius (e.g. Igumenshchev 2009). Since accretion within the magnetospheric radius proceeds through RTI modes, we expect that the power spectrum of the Comptonized emission from the corona will differ substantially from the outer disk's blackbody emission. In future work we will address how the cold-phase gas transitions into hot-phase gas in the corona. At the moment of writing, we suspect that magnetic reconnection in equatorial current sheets heats a small fraction of the cold-phase gas to extremely high temperatures, which becomes the hot-phase, while leaving most of the cold-phase gas unaffected.

Spectral state transitions (e.g., Fender et al. 2004a) can potentially be explained by the outwards diffusion of magnetic flux through the disk on timescales orders of magnitude longer than the duration of our simulations (e.g. Lubow et al.

1994; Begelman & Armitage 2014). From an observational perspective, the truncation radius needs to move inwards to explain the softening of the spectrum during a hard-to-soft state transition (e.g. Esin et al. 1997) while the magnetic flux needs to diffuse out to explain the lack of any jets in the high-soft state (e.g. Fender et al. 2004a). It is conceivable that outwards diffusion of the magnetic flux in our model will progressively reduce the magnetic truncation radius, which will cause the spectrum to become softer. However, even when the entire disk leaves the MAD state, residual large scale poloidal magnetic flux might still be present and launch powerful winds from the inner disk. Such winds could be significantly hotter compared to the winds in RADTOR and could potentially explain the hard emission tail observed in the soft (-intermediate) states of BHXRBs, which might be associated with a corona that sandwiches the accretion disk. We will explore this possibility in future work.

While our radiative two-temperature GRMHD simulations have modeled from first principles the structure of the corona and pinpointed possible locations for the origin of the photons (via direct emission and Comptonization), they have not yet established that our simulated corona will indeed reproduce the spectra associated with the hard-intermediate state in BHXRBs. Ray-tracing of the simulation data (e.g. Krawczynski 2021) will be able to place unique constraints on the emission from our model and quantify the relative contributions of the cold-phase and hot-phase gas both to the direct emission of seed photons and to Comptonization. However, this will face several challenges. For example, magnetic reconnection in collisionless plasma leads to the formation of non-thermal particle populations (e.g. Sironi & Spitkovsky 2014; Beloborodov 2017; Sironi & Beloborodov 2020; Sridhar et al. 2021). Since ideal GRMHD is unable to model the full energy distribution of such particles, deviation from the

thermal spectrum is a free parameter that should be quantified by future particle-in-cell (PIC) simulations. In addition, it is likely that there are some inaccuracies in the electron temperatures presented in this work. These stem from the intrinsic challenges associated with quantifying the dissipation rate in a highly magnetized plasma, and from the inherent limitations related to our two-moment (M1) radiation scheme, which works best in regions of high optical depth where emission and scattering of photons is localized. We will address these and other uncertainties in future work.

## 6. ACKNOWLEDGEMENTS

We thank Michiel van der Klis, Adam Ingram, Sera Markoff, Ramesh Narayan, and Eliot Quataert for insightful discussions. An award of computer time was provided by the Innovative and Novel Computational Impact on Theory and Experiment (INCITE) program under award PHY129. This research used resources of the Oak Ridge Leadership Computing Facility, which is a DOE Office of Science User Facility supported under Contract DE-AC05-00OR22725. This research also used HPC and visualization resources provided by the Texas Advanced Computing Center (TACC) at The University of Texas at Austin, which contributed to our results via the LRAC allocation AST20011 and through Texascale Days (<http://www.tacc.utexas.edu>). We acknowledge PRACE for awarding us access to JUWELS Booster at GCS@JSC, Germany. ML was supported by the John Harvard Distinguished Science Fellowship, GM is supported by a Netherlands Research School for Astronomy (NOVA), Virtual Institute of Accretion (VIA) postdoctoral fellowship and AT by the National Science Foundation grants AST-2009884, AST-1815304 and AST-1911080.

## REFERENCES

- Abramowicz M. A., Fragile P. C., 2013, *Living Reviews in Relativity*, 16, 1
- Begelman M. C., Armitage P. J., 2014, *ApJL*, 782, L18
- Begelman M. C., Pringle J. E., 2007, *MNRAS*, 375, 1070
- Begelman M. C., Scepi N., Dexter J., 2021, arXiv e-prints, p. arXiv:2111.02439
- Beloborodov A. M., 1999, *ApJL*, 510, L123
- Beloborodov A. M., 2017, *ApJ*, 850, 141
- Colella P., Woodward P. R., 1984, *Journal of Computational Physics*, 54, 174
- Davis S. W., Tchekhovskoy A., 2020, *ARA&A*, 58, 407
- Del Santo M., Malzac J., Belmont R., Bouchet L., De Cesare G., 2013, *MNRAS*, 430, 209
- Dexter J., Scepi N., Begelman M. C., 2021, *ApJL*, 919, L20
- Done C., Gierliński M., 2006, *MNRAS*, 367, 659
- Done C., Gierliński M., Kubota A., 2007, *A&A Rv*, 15, 1
- Esin A. A., McClintock J. E., Narayan R., 1997, *ApJ*, 489, 865
- Fanaroff B. L., Riley J. M., 1974, *MNRAS*, 167, 31P
- Fender R. P., Belloni T. M., Gallo E., 2004a, *MNRAS*, 355, 1105
- Fender R. P., Belloni T. M., Gallo E., 2004b, *MNRAS*, 355, 1105
- Ferreira J., Petrucci P. O., Henri G., Saugé L., Pelletier G., 2006, *A&A*, 447, 813
- Fishbone L. G., Moncrief V., 1976, *ApJ*, 207, 962
- Fukumura K., Kazanas D., 2007, *ApJ*, 664, 14
- Gardiner T. A., Stone J. M., 2005, *Journal of Computational Physics*, 205, 509
- Igumenshchev I. V., 2008, *ApJ*, 677, 317
- Igumenshchev I. V., 2009, *ApJL*, 702, L72

- Igumenshchev I. V., Narayan R., Abramowicz M. A., 2003, *ApJ*, 592, 1042
- Ingram A., Done C., Fragile P. C., 2009, *MNRAS*, 397, L101
- Kara E., et al., 2019, *Nature*, 565, 198
- Krawczynski H., 2021, *ApJ*, 906, 34
- Lančová D., et al., 2019, *ApJL*, 884, L37
- Lightman A. P., Eardley D. M., 1974, *ApJL*, 187, L1
- Liska M., Tchekhovskoy A., Ingram A., van der Klis M., 2018a, preprint, ([arXiv:1810.00883](https://arxiv.org/abs/1810.00883))
- Liska M., Hesp C., Tchekhovskoy A., Ingram A., van der Klis M., Markoff S., 2018b, *MNRAS*, 474, L81
- Liska M., et al., 2019, arXiv e-prints, p. [arXiv:1912.10192](https://arxiv.org/abs/1912.10192)
- Liu X.-D., Osher S., 1998, *Journal of Computational Physics*, 142, 304
- Lubow S. H., Papaloizou J. C. B., Pringle J. E., 1994, *Monthly Notices of the Royal Astronomical Society*, 267, 235
- Marcel G., et al., 2018, *A&A*, 615, A57
- Markoff S., Nowak M. A., Wilms J., 2005, *ApJ*, 635, 1203
- McKinney J. C., Tchekhovskoy A., Blandford R. D., 2012, *MNRAS*, 423, 3083
- McKinney J. C., Tchekhovskoy A., Blandford R. D., 2013, *Science*, 339, 49
- McKinney J. C., Chluba J., Wielgus M., Narayan R., Sądowski A., 2017, *MNRAS*, 467, 2241
- Meyer F., Meyer-Hofmeister E., 1994, *A&A*, 288, 175
- Meyer-Hofmeister E., Meyer F., 2011, *A&A*, 527, A127
- Morales Teixeira D., Avara M. J., McKinney J. C., 2018, *MNRAS*, 480, 3547
- Narayan R., Igumenshchev I. V., Abramowicz M. A., 2003, *PASJ*, 55, L69
- Narayan R., Yi I., 1994, *ApJL*, 428, L13
- Noble S. C., Krolik J. H., Hawley J. F., 2009, *ApJ*, 692, 411
- Novikov I. D., Thorne K. S., 1973, in Dewitt C., Dewitt B. S., eds, *Black Holes (Les Astres Occlus)*. pp 343–450
- Porth O., et al., 2019, *ApJS*, 243, 26
- Qian L., Liu B. F., Wu X.-B., 2007, *The Astrophysical Journal*, 668, 1145
- Reis R. C., Fabian A. C., Miller J. M., 2010, *MNRAS*, 402, 836
- Remillard R. A., McClintock J. E., 2006, *ARA&A*, 44, 49
- Ressler S. M., Tchekhovskoy A., Quataert E., Chandra M., Gammie C. F., 2015, *MNRAS*, 454, 1848
- Ressler S. M., Tchekhovskoy A., Quataert E., Gammie C. F., 2017, *MNRAS*, 467, 3604
- Reynolds C. S., Fabian A. C., 1997, *MNRAS*, 290, L1
- Ripperda B., Liska M., Chatterjee K., Musoke G., Philippov A. A., Markoff S. B., Tchekhovskoy A., Younsi Z., 2021, [arXiv:2109.15115](https://arxiv.org/abs/2109.15115) [astro-ph, physics:gr-qc, physics:physics]
- Rowan M. E., Sironi L., Narayan R., 2017, *ApJ*, 850, 29
- Rybicki G. B., Lightman A. P., 1986, *Radiative Processes in Astrophysics*
- Sądowski A., Narayan R., Tchekhovskoy A., Zhu Y., 2013, *MNRAS*, 429, 3533
- Sądowski A., 2016, *MNRAS*, 459, 4397
- Sądowski A., Narayan R., 2015, *MNRAS*, 454, 2372
- Sądowski A., Wielgus M., Narayan R., Abarca D., McKinney J. C., Chael A., 2017, *MNRAS*, 466, 705
- Scepi N., Begelman M. C., Dexter J., 2021, *MNRAS*, 502, L50
- Shakura N. I., Sunyaev R. A., 1973, *A&A*, 24, 337
- Shakura N. I., Sunyaev R. A., 1976, *MNRAS*, 175, 613
- Sironi L., Beloborodov A. M., 2020, *ApJ*, 899, 52
- Sironi L., Spitkovsky A., 2014, *ApJ*, 783, L21
- Sridhar N., Sironi L., Beloborodov A. M., 2021, *MNRAS*, 507, 5625
- Tchekhovskoy A., 2015, in Contopoulos I., Gabuzda D., Kylafis N., eds, *Astrophysics and Space Science Library Vol. 414, The Formation and Disruption of Black Hole Jets*. p. 45, [doi:10.1007/978-3-319-10356-3\\_3](https://doi.org/10.1007/978-3-319-10356-3_3)
- Tchekhovskoy A., Narayan R., McKinney J. C., 2011, *MNRAS*, 418, L79
- Volonteri M., Sikora M., Lasota J.-P., 2007, *ApJ*, 667, 704
- Wardziński G., Zdziarski A. A., 2000, *MNRAS*, 314, 183
- Wilkins D. R., Fabian A. C., 2012, *MNRAS*, 424, 1284